UDC 621.039.51

Badawi M.S., Gouda M.M., El-Khatib A.M., Nafee S.S., El-Mallah E.A.
Physics Department, Faculty of Science, Alexandria University, 21511 Alexandria, Egypt

NEW ANALYTICAL APPROACH TO CALIBRATE CYLINDRICAL HPGE DETECTOR INCLUDING CORRECTIONS FOR SELF ATTENUATION OF LARGE CYLINDRICAL SOURCES AND ATTENUATION OF ALL DETECTOR HOUSING MATERIALS

HPGe semiconductor detectors are very useful for radioactivity measurement and to calculate the absolute activity, the full energy peak efficiency of the detector is needed. In this work, to calibrate the co-axial HPGe semiconductor detector, we introduce a new theoretical approach based on the Direct Statistical method proposed by Selim and Abbas to calculate the full-energy peak efficiency for cylindrical detectors. The present method depends on the accurate analytical calculation of the average path length covered by the photon inside the detector active volume and the geometrical solid angle, Щ, to obtain a simple formula for the efficiency. In addition, self attenuation of source matrix (with radius greater than the radius of the detector), the attenuation by the source container and the detector housing materials are also treated by calculating the average path length cross these materials. 152 Eu aqueous sources covering the energy range from 121 up to 1408 keV were used. Remarkable agreement between the measured and the calculated efficiencies is achieved with discrepancies less than 2%.

Keywords: HPGe detectors, large cylindrical sources, full-energy peak efficiency and self-attenuation.

1. Introduction

For low activity samples, using the extended sources in gamma ray spectrometry will improve the sensitivity of detection and in order to obtain correct results, the self attenuation of the sample must be taken into consideration. The calculation of full-energy peak efficiency and the self attenuation of source material using experimental, semi-empirical and Monte Carlo approaches have been treated by several authors (Lippert, 1983; Moens and Hoste, 1983; Nakamura, 1983; Haase et al., 1993; Mihaljevic et al., 1993; Wang et al., 1995; Sima and Arnold, 1996 and Wang et al., 1997). Recently, Selim and Abbas (1998, 2000); Abbas (2001a, 2001b, 2001c); Abbas and Selim (2002), using spherical coordinates system, derived direct analytical integrals of the detector efficiencies (total and full-energy peak) for any source-detector configuration and implemented these analytical expressions into a numerical integration computer program. Moreover, they introduced a new theoretical approach (Abbas, 2006; Abbas et al., 2006; Nafee and Abbas, 2008) based on that Direct Statistical method to determine the detector efficiency for an isotropic radiating point source at any arbitrary position from a cylindrical detector, as well as the extension of this approach to evaluate the volumetric sources.

In the present work, we will modify this simplified approach to determine the full-energy peak efficiency of the co-axial detector with respect to point and volumetric sources, taking into account evaluating the attenuation f_{att} by the dead layer and the end-cap material of the detector, the self attenuation S_{self} by the source matrix and finally, the attenuation S_{sc} by the source container material.

The arrangement of this paper is as follows. Section 2 presents direct mathematical formulae for the full-energy peak efficiency for the point source and the large cylindrical source, where the attenuation of photons through the dead layer, the detector end cap material, the source container material and through the source itself is also treated. Section 3 contains experimental setup used in our measurements. Section 4 contains comparisons between the calculated efficiency using the formulae derived in this work with the experimental measurements to show the validity of the present mathematical formulae. Conclusions are presented in Section 5.

2. Mathematical viewpoint

2.1. The case of a non-axial point source

Consider a right circular cylindrical (2R x L), detector and an arbitrarily positioned isotropic radiating point source located at a distance h from the detector top surface, and at a lateral distance ρ from its axis. The efficiency of the detector with respect to point source is given as follows (Abbas et al., 2006):

$$\varepsilon_{po\,\mathrm{int}} = f_{att}\,\varepsilon_g\,\varepsilon_i \qquad (1)$$

where ε_i and ε_g are the intrinsic and the geometrical efficiencies which were derived by Abbas et al., (2006) and it is very important to reintroduce in Section 2.1.1 because they are essential in the present work. f_{att} is the attenuation by the detector dead layer and end cap material and in Section 2.1.2, this factor will be calculated by a new method which is dependent on calculating the average path length cross these materials.

2.1.1. The intrinsic (ε_i) and the geometrical (ε_g) efficiencies

The intrinsic and geometrical efficiencies are represented by Eqs. (2) and (3) respectively.

$$\varepsilon_i = 1 - e^{-\mu \bar{d}} \qquad (2)$$

$$\varepsilon_g = \frac{\text{Ш}}{4\pi} \qquad (3)$$

where $\bar{d}$ is the average path length traveled by a photon through the detector, Ш is the solid angle subtended by the source-detector and they are represented by Eqs. (4) and (5) respectively, and they will be discussed in details according to the source detector configuration as shown below, while μ is the attenuation coefficient of the detector material.

$$\bar{d} = \frac{\int_{\Omega} (\sum_{j} d_j d\Omega)}{\int_{\Omega} d\Omega} = \frac{\int_{\theta}\int_{\varphi} (\sum_{j=1}^{n} d_j) \sin\theta d\varphi d\theta}{\Omega} \qquad (4)$$

where d_1, d_2, ..., d_n are the possible path lengths traveled by the photon within the detector active volume.

$$\Omega = \int_{\theta}\int_{\varphi} \sin\theta\, d\theta\, d\varphi\,. \qquad (5)$$

There are two main cases to be considered for calculating the efficiency of the detector with respect to point source, the first is that the lateral displacement of the source is smaller than or equal the detector circular face's radius ($\rho \le R$) and the second is that the lateral distance of the source is greater than the detector circular face's radius ($\rho > R$). The two cases have been treated by Abbas et al., (2006). Table 1 shows the geometrical efficiency, the possible path lengths and the average path length traveled by the photon within the detector active volume for both cases. The values of the polar and the azimuthal angles are shown in Table 2.

2.1.2. The attenuation factor (f_{att})

The attenuation factor f_{att} is expressed as:

$$f_{att} = f_{lay}\, f_{cap} \qquad (6)$$

where f_{lay} is the attenuation by the detector dead layer and f_{cap} is the attenuation by the detector end cap material and they are given by:

$$f_{lay} = e^{-\mu_{lay}\,\overline{\delta_{lay}}} \quad , \quad f_{cap} = e^{-\mu_{cap}\,\overline{\delta_{cap}}} \qquad (7)$$

where μ_{lay} and μ_{cap} are the attenuation coefficients of the detector dead layer and end cap material respectively. While $\overline{\delta_{lay}}$ and $\overline{\delta_{cap}}$ are the average path length traveled by a photon through the detector dead layer and end cap material respectively and they are represented as follow:

$$\left.\begin{aligned} \overline{\delta_{lay}} &= \frac{\int_{\varphi}\int_{\theta}\sum_{j=1}^{n} t'_j \sin\theta\, d\theta\, d\varphi}{\int_{\varphi}\int_{\theta} \sin\theta\, d\theta\, d\varphi} = \frac{\int_{\varphi}\int_{\theta}\sum_{j=1}^{n} t'_j \sin\theta\, d\theta\, d\varphi}{\Omega} \\ \overline{\delta_{cap}} &= \frac{\int_{\varphi}\int_{\theta}\sum_{j=1}^{n} t''_j \sin\theta\, d\theta\, d\varphi}{\int_{\varphi}\int_{\theta} \sin\theta\, d\theta\, d\varphi} = \frac{\int_{\varphi}\int_{\theta}\sum_{j=1}^{n} t''_j \sin\theta\, d\theta\, d\varphi}{\Omega} \end{aligned}\right\} \qquad (8)$$

where, $t'_1, t'_2, \ldots, t'_n$ and $t''_1, t''_2, \ldots, t''_n$ are the possible path lengths traveled by the photon within the detector dead layer and end cap material respectively.

The case in which $\rho \le R$

Consider the detector has dead layer with upper surface thickness t_{DF}. Each photon enters the detector must pass through the face of dead layer, so that there is only one photon path length through the dead layer which is given by:

$$t'_1 = \frac{t_{DF}}{\cos\theta}\,. \qquad (9)$$

The average path length $\overline{\delta_{lay}}$ traveled by a photon through the dead layer is given by:

$$\overline{\delta_{lay}} = \frac{Z_1}{I_2} \qquad (10)$$

where I_2 is as identified before in Table 1 and Z_1 is given by:

Table 1. The geometrical efficiency, the possible path lengths and the average path length traveled by the photon within the detector active volume for cases $c \le R$ and $c > R$ (Abbas et al., 2006)

<table>
<tr><th>$\rho > R$</th><th>$\rho \le R$</th></tr>
<tr><td>

$$d_1 = \frac{L}{\cos\theta} \quad \textbf{(face} \rightarrow \textbf{base)}$$

$$d_2 = \frac{\rho\cos\varphi + \Delta\sqrt{R^2 - \rho^2\sin^2\varphi}}{\sin\theta} - \frac{h}{\cos\theta} \quad \textbf{(face} \rightarrow \textbf{side)}$$

$$d_3 = \frac{h+L}{\cos\theta} - \frac{\rho\cos\varphi + \Delta\sqrt{R^2 - \rho^2\sin^2\varphi}}{\sin\theta} \quad \textbf{(side} \rightarrow \textbf{base)}$$

$$d_4 = \frac{2\sqrt{R^2 - \rho^2\sin^2\varphi}}{\sin\theta} \quad \textbf{(side} \rightarrow \textbf{side),}$$

$$\Delta = \begin{cases} -1 & \theta < \theta_T \\ 1 & \theta \ge \theta_T \end{cases} \qquad \bar{d} = \frac{I_3}{I_4} \;, \quad \varepsilon_g = \frac{I_4}{2\pi}$$

</td><td>

$$d_1 = \frac{L}{\cos\theta} \quad \textbf{(face} \rightarrow \textbf{base)}$$

$$d_2 = \frac{\rho\cos\varphi + \sqrt{R^2 - \rho^2\sin^2\varphi}}{\sin\theta} - \frac{h}{\cos\theta} \quad \textbf{(face} \rightarrow \textbf{side)}$$

$$\bar{d} = \frac{I_1}{I_2} \;, \quad \varepsilon_g = \frac{I_2}{2\pi}$$

</td></tr>
<tr><td>

$$I_3 = \int_{\theta_1}^{\theta_2}\int_0^{\varphi'_{\max}} d_3 \sin\theta\, d\varphi\, d\theta + \int_{\theta_2}^{\theta_T}\left(\int_0^{\varphi_{\max}} d_1 \sin\theta\, d\varphi + \int_{\varphi_{\max}}^{\varphi'_{\max}} d_3 \sin\theta\, d\varphi\right) d\theta$$
$$+ \int_{\theta'_c}^{\theta_T}\int_{\varphi_{\max}}^{\varphi_c} d_4 \sin\theta\, d\varphi\, d\theta + \int_{\theta_T}^{\theta_3}\left(\int_0^{\varphi'_{\max}} d_1 \sin\theta\, d\varphi + \int_{\varphi_{\max}}^{\varphi_{\max}} d_2 \sin\theta\, d\varphi\right) d\theta$$
$$+ \int_{\theta_T}^{\theta_c}\int_{\varphi_{\max}}^{\varphi_c} d_4 \sin\theta\, d\varphi\, d\theta + \int_{\theta_3}^{\theta_4}\int_0^{\varphi_{\max}} d_2 \sin\theta\, d\varphi\, d\theta \qquad (\theta_3 \ge \theta_2)$$

$$I_3 = \int_{\theta_1}^{\theta_3}\int_0^{\varphi'_{\max}} d_3 \sin\theta\, d\varphi\, d\theta + \int_{\theta'_c}^{\theta_2}\int_{\varphi'_{\max}}^{\varphi_c} d_4 \sin\theta\, d\varphi\, d\theta$$
$$+ \int_{\theta_3}^{\theta_2}\int_0^{\varphi_c} d_4 \sin\theta\, d\varphi\, d\theta$$
$$+ \int_{\theta_2}^{\theta_c}\int_{\varphi_{\max}}^{\varphi_c} d_4 \sin\theta\, d\varphi\, d\theta + \int_{\theta_2}^{\theta_4}\int_0^{\varphi_{\max}} d_2 \sin\theta\, d\varphi\, d\theta \qquad (\theta_3 < \theta_2)$$

$$I_4 = \int_{\theta_1}^{\theta'_c} \varphi'_{\max} \sin\theta\, d\theta + \int_{\theta'_c}^{\theta_c} \varphi_c \sin\theta\, d\theta + \int_{\theta_c}^{\theta_4} \varphi_{\max} \sin\theta\, d\theta$$

</td><td>

$$I_1 = \pi \int_0^{\theta_1} d_1 \sin\theta\, d\theta + \int_{\theta_1}^{\theta_2}\int_0^{\pi} d_2 \sin\theta\, d\varphi\, d\theta$$
$$+ \int_{\theta_2}^{\theta_4}\int_0^{\varphi_{\max}} d_2 \sin\theta\, d\varphi\, d\theta$$
$$+ \int_{\theta_1}^{\theta_3}\left[\varphi'_{\max} d_1 \sin\theta - \int_0^{\varphi'_{\max}} d_2 \sin\theta\, d\varphi\right] d\theta$$

$$I_2 = \pi \int_0^{\theta_2} \sin\theta\, d\theta + \int_{\theta_2}^{\theta_4} \varphi_{\max} \sin\theta\, d\theta$$

</td></tr>
<tr><td>

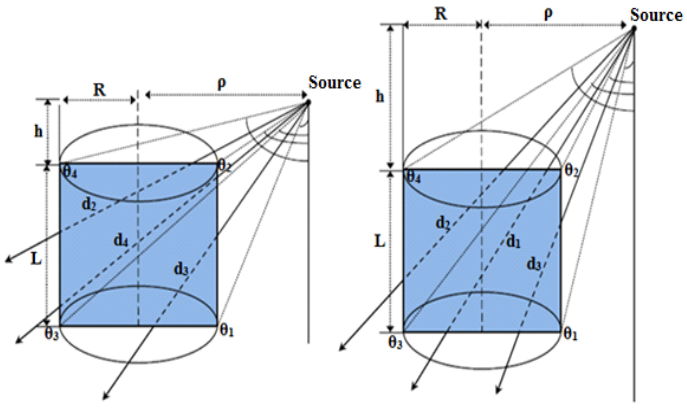

</td><td>

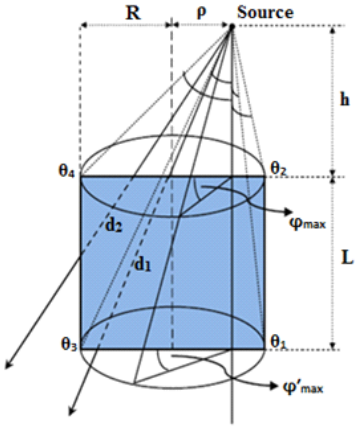

</td></tr>
</table>

$$Z_1 = \int_0^{\pi}\int_0^{\theta_2} t_1' \sin\theta \, d\theta \, d\varphi + \int_0^{\varphi_{\max}}\int_{\theta_2}^{\theta_4} t_1' \sin\theta \, d\theta \, d\varphi \,. \quad (11)$$

Also, if t_a is the thickness of upper surface of end cap material, so, each photon to enter the detector must pass through the face of end cap, so that there is only one photon path length through the end cap which is given by:

$$t_1'' = \frac{t_a}{\cos\theta} \,. \quad (12)$$

The average path length $\overline{\delta_{cap}}$ traveled by a photon through end cap is given by:

$$\overline{\delta_{cap}} = \frac{Z_1'}{I_2} \quad (13)$$

where I_2 is as identified before in Table 1 and Z_1' is given by:

$$Z_1' = \int_0^{\pi}\int_0^{\theta_2} t_1'' \sin\theta \, d\theta \, d\varphi + \int_0^{\varphi_{\max}}\int_{\theta_2}^{\theta_4} t_1'' \sin\theta \, d\theta \, d\varphi \,. \quad (14)$$

The case in which ρ>R

For dead layer of the detector with upper surface thickness t_{DF} and side surface thickness t_{DS}, as shown in Fig. 1, there are two probabilities to be considered for the photon path length to pass through dead layer and enter the detector as follow:

I. From the face of dead layer, so that the photon path length through dead layer is given by:

$$t_1' = \frac{t_{DF}}{\cos\theta} \,. \quad (15)$$

II. From the side of dead layer, so that the photon path length through dead layer is given by:

$$t_2' = \frac{\rho\cos\varphi + \sqrt{\left(R + t_{DS}\right)^2 - \rho^2 \sin^2\varphi}}{\sin\theta} - \frac{\rho\cos\varphi + \sqrt{(R)^2 - \rho^2\sin^2\varphi}}{\sin\theta} \cong \frac{t_{DS}\left(1 + \frac{\rho^2}{2R^2}\sin^2\varphi\right)}{\sin\theta} \quad (16)$$

The average path length $\overline{\delta_{lay}}$ traveled by a photon through the dead layer is given by:

$$\overline{\delta_{lay}} = \frac{Z_3}{I_4} \quad (17)$$

where I_4 is as identified before in Table 1, while, there are two sub cases for obtaining the value of Z_3 according to the values of the polar angles θ_i as follow:

i. The case in which ($\theta_2 \geq \theta_c'$)

$$Z_3 = \int_{\theta_1}^{\theta_c'}\int_0^{\varphi_{\max}'} t_2' \sin\theta \, d\varphi \, d\theta + \int_{\theta_c'}^{\theta_2}\int_0^{\varphi_c} t_2' \sin\theta \, d\varphi \, d\theta + \int_{\theta_2}^{\theta_c}\int_0^{\varphi_c} t_1' \sin\theta \, d\varphi \, d\theta + \int_{\theta_c}^{\theta_4}\int_0^{\varphi_{\max}} t_1' \sin\theta \, d\varphi \, d\theta \,. \quad (18)$$

ii. The case in which ($\theta_2 < \theta_c'$)

$$Z_3 = \int_{\theta_1}^{\theta_2}\int_0^{\varphi_{\max}'} t_2' \sin\theta \, d\varphi \, d\theta + \int_{\theta_2}^{\theta_c'}\int_0^{\varphi_{\max}'} t_1' \sin\theta \, d\varphi \, d\theta + \int_{\theta_c'}^{\theta_c}\int_0^{\varphi_c} t_1' \sin\theta \, d\varphi \, d\theta + \int_{\theta_c}^{\theta_4}\int_0^{\varphi_{\max}} t_1' \sin\theta \, d\varphi \, d\theta \,. \quad (19)$$

Table 2. The values of the polar and the azimuthal angles based on the source to detector configuration (Abbas et al., 2006)

The azimuthal angles	The polar angles
$\theta_1 = \tan^{-1}\left(\frac{\lvert R-\rho\rvert}{h+L}\right)$, $\theta_2 = \tan^{-1}\left(\frac{\lvert R-\rho\rvert}{h}\right)$, $\theta_3 = \tan^{-1}\left(\frac{R+\rho}{h+L}\right)$,	$\varphi_{\max} = \cos^{-1}\left(\frac{\rho^2 - R^2 + h^2\tan^2\theta}{2\rho h\tan\theta}\right)$
$\theta_4 = \tan^{-1}\left(\frac{R+\rho}{h}\right)$, $\theta_c = \tan^{-1}\left(\frac{\sqrt{\rho^2-R^2}}{h+L}\right)$, $\theta_c' = \tan^{-1}\left(\frac{\sqrt{\rho^2-R^2}}{h}\right)$,	$\varphi_{\max}' = \cos^{-1}\left(\frac{\rho^2 - R^2 + (h+L)^2\tan^2\theta}{2\rho(h+L)\tan\theta}\right)$
$\theta_T = \tan^{-1}\left(\frac{\sqrt{\rho^2-R^2}}{\sqrt{h(h+L)}}\right)$, $(\varphi_{\max} = \varphi_{\max}')$	$\varphi_c = \sin^{-1}\left(\frac{R}{\rho}\right)$

Consider end cap material of upper surface thickness t_a , side surface thickness t_w, and inner radius R_a, as shown in Fig. 1, there are two cases considered according to the relation between the lateral distance ρ, and the inner radius of the detector end cap as follow:

a) the case in which $(R < \rho \le R_a)$

In this case we can see that, each photon to enter the detector must pass through the face of end cap, so that there is only one photon path length through the end cap which is given by:

$$t_1'' = \frac{t_a}{\cos\theta}; \qquad (20)$$

b) the case in which $(\rho > R_a)$

In this case there is very important polar angle must be taken into consideration which is θ_{cap}, and is given by:

$$\theta_{cap} = \tan^{-1}\left(\frac{\rho - R_a}{h - k}\right) \qquad (21)$$

where k is the distance between the detector end cap and the detector upper surface.

There are two probabilities to be considered for the photon path length to pass through end cap and enter the detector as follow:

I. From the face of end cap, so that the photon path length through end cap is given by:

$$t_1'' = \frac{t_a}{\cos\theta}; \qquad (22)$$

II. From the side of end cap, so that the photon path length through end cap is given by:

$$t_2'' = \frac{\rho\cos\varphi + \sqrt{(R_a + t_w)^2 - \rho^2\sin^2\varphi}}{\sin\theta} - \frac{\rho\cos\varphi + \sqrt{(R_a)^2 - \rho^2\sin^2\varphi}}{\sin\theta} \cong \frac{t_w\left(1 + \frac{\rho^2}{2R_a^2}\sin^2\varphi\right)}{\sin\theta}. \qquad (23)$$

The average path length $\overline{\delta_{cap}}$ traveled by a photon through end cap is given by:

$$\overline{\delta_{cap}} = \frac{Z_3'}{I_4} \qquad (24)$$

where I_4 is as identified before in Table 1, while Z_3' is varied according to the possible relations between the polar angles for two main previous cases. Table 3 shows the values of Z_3'.

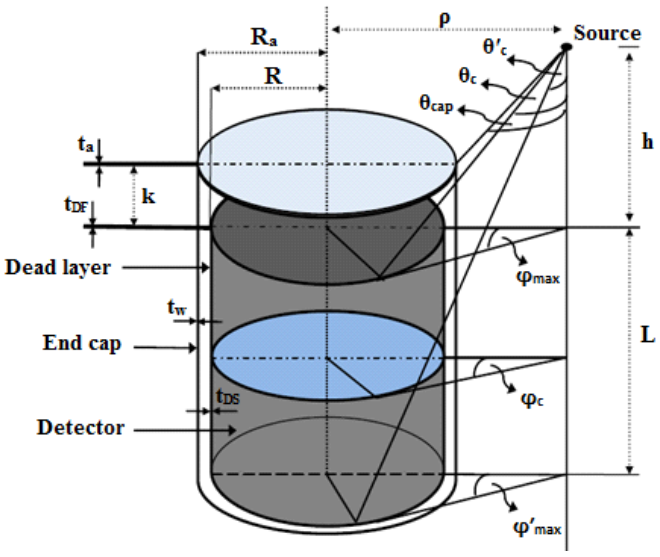

Fig. 1. A diagram of a cylindrical – type detector with a non-axial point source (ρ >R)

2.2. The case of a co-axial cylindrical source

The efficiency of a cylindrical detector with radius R and height L arising from a cylindrical source with radius S (S>R) and height H, as shown in Fig. 2, is given by:

$$\varepsilon_{cyl} = \frac{S_{self}\, S_{sc}\, f_{att}\, \varepsilon_i\, \varepsilon_g}{V} \qquad (25)$$

where V is the volume of the cylindrical source (V=pS^{2}H), S_{self} is the self attenuation by the source matrix and S_{sc} is the attenuation by the source container material. The intrinsic and geometrical efficiencies are as identified before in Eqs. (2) and (3) respectively, but the average path length $\overline{d}$ traveled by the photon through the detector active volume and the solid angle will have new forms due to the geometry of the volumetric source, as shown in Fig. 2. The average path length is expressed as:

$$\overline{d} = \frac{\int_{h_o}^{H+h_o}\int_0^{2\pi}\left(\int_0^R I_1\,\rho\,d\rho + \int_R^S I_3\,\rho\,d\rho\right)d\alpha\,dh}{\int_{h_o}^{H+h_o}\int_0^{2\pi}\left(\int_0^R I_2\,\rho\,d\rho + \int_R^S I_4\,\rho\,d\rho\right)d\alpha\,dh} \qquad (26)$$

where α is the angle between the lateral dis-

tance ρ and the detector's major axis. The geometrical efficiency ε_g is given by:

$$\varepsilon_g = \frac{\int_{h_o}^{H+h_o}\int_{0}^{2\pi}\left(\int_{0}^{R} I_2\,\rho\,d\rho + \int_{R}^{S} I_4\,\rho\,d\rho\right)d\alpha\,dh}{2\pi} \quad (27)$$

where I_1, I_2, I_3 and I_4 are as identified before in Table 1.

The new forms of the average path length traveled by the photon through the detector dead layer and the detector end cap material are given by Eqs. (28) and (29) respectively.

$$\overline{\delta_{lay}} = \frac{\int_{h_o}^{H+h_o}\int_{0}^{2\pi}\left(\int_{0}^{R} Z_1\,\rho\,d\rho + \int_{R}^{S} Z_3\,\rho\,d\rho\right)d\alpha\,dh}{\int_{h_o}^{H+h_o}\int_{0}^{2\pi}\left(\int_{0}^{R} I_2\,\rho\,d\rho + \int_{R}^{S} I_4\,\rho\,d\rho\right)d\alpha\,dh} \quad (28)$$

where Z_1 is as identified before in Eq. (11),while Z_3 represented by Eqs. (18) or (19) according to the values of the polar angles θ_i.

$$\overline{\delta_{cap}} = \frac{\int_{h_o}^{H+h_o}\int_{0}^{2\pi}\left(\int_{0}^{R} Z_1'\,\rho\,d\rho + \int_{R}^{S} Z_3'\,\rho\,d\rho\right)d\alpha\,dh}{\int_{h_o}^{H+h_o}\int_{0}^{2\pi}\left(\int_{0}^{R} I_2\,\rho\,d\rho + \int_{R}^{S} I_4\,\rho\,d\rho\right)d\alpha\,dh} \quad (29)$$

where Z_1' is as identified before in Eq. (11),while Z_3' is as identified before in Table 3.

In the case of a co-axial cylindrical source with radius is greater than the radius of the detector, there are two probabilities to be considered; the probability that the lateral distance of the source is smaller than the detector circular face radius, i.e. $\rho \le$R and the lateral distance of the source is greater than the detector circular face radius, i.e. $\rho >$R and in the two cases, there is only one path to the photon that way out from the source which is exit from the base and is given by:

$$t_1 = \frac{h - h_o}{\cos\theta} \quad (30)$$

where h_o is the distance between the source active volume and the detector upper surface. The source matrix self attenuation S_{self} is given by:

$$S_{self} = e^{-\mu_s \bar{t}} \quad (31)$$

where μ_s is the attenuation coefficient of the source matrix and $\bar{t}$ is the average path length traveled by a photon inside the source and is given by:

$$\bar{t} = \bar{t}(t_1) = \frac{\int_{h_o}^{h_o+H}\int_{0}^{\pi}\int_{0}^{R} g_1\,\rho\,d\rho\,d\alpha\,dh + \int_{h_o}^{h_o+H}\int_{0}^{\pi}\int_{R}^{S} g_2\,\rho\,d\rho\,d\alpha\,dh}{\int_{h_o}^{h_o+H}\int_{0}^{\pi}\int_{0}^{R} I_2\,\rho\,d\rho\,d\alpha\,dh + \int_{h_o}^{h_o+H}\int_{0}^{\pi}\int_{R}^{S} I_4\,\rho\,d\rho\,d\alpha\,dh} \quad (32)$$

where:

$$g_1 = \pi\int_{0}^{\theta_2} t_1 \sin\theta\,d\theta + \int_{\theta_2}^{\theta_4} \varphi_{\max}\, t_1 \sin\theta\,d\theta \quad (33)$$

$$\begin{aligned} g_2 &= \int_{\theta_1}^{\theta_c'}\int_{0}^{\varphi'_{\max}} t_1 \sin\theta\,d\varphi\,d\theta + \int_{\theta_c'}^{\theta_c}\int_{0}^{\varphi_c} t_1 \sin\theta\,d\varphi\,d\theta + \int_{\theta_c}^{\theta_4}\int_{o}^{\varphi_{\max}} t_1 \sin\theta\,d\varphi\,d\theta \\ &= \int_{\theta_1}^{\theta_c'} \varphi'_{\max} t_1 \sin\theta\,d\theta + \int_{\theta_c'}^{\theta_c} \varphi_c\, t_1 \sin\theta\,d\theta + \int_{\theta_c}^{\theta_4} \varphi_{\max} t_1 \sin\theta\,d\theta \end{aligned} \quad (34)$$

If t_B is the source container bottom thickness, so, there is only one path to the photon that way out from the source container which is exit from the base and is given by:

$$t_1''' = \frac{t_B}{\cos\theta}. \quad (35)$$

The attenuation S_{sc} by the source container material is given by:

$$S_{sc} = e^{-\mu_c \bar{t}_c} \quad (36)$$

where μ_c is the attenuation coefficient of the source

Table 3. The different integration terms for Z_3' according to the possible relations between the polar angles for cases $R < c \le R_a$ and $c > R_a$

	Z_3'	
	$\int_{\theta_1}^{\theta_c'}\int_{0}^{\varphi_{\max}'} t_1'' \sin\theta d\varphi d\theta + \int_{\theta_c'}^{\theta_c}\int_{0}^{\varphi_c} t_1'' \sin\theta d\varphi d\theta + \int_{\theta_c}^{\theta_4}\int_{0}^{\varphi_{\max}} t_1'' \sin\theta d\varphi d\theta$	$R < \rho \le R_a$
$\theta_1 \ge \theta_{cap}$	$\int_{\theta_1}^{\theta_c'}\int_{0}^{\varphi_{\max}'} t_1'' \sin\theta d\varphi d\theta + \int_{\theta_c'}^{\theta_c}\int_{0}^{\varphi_c} t_1'' \sin\theta d\varphi d\theta + \int_{\theta_c}^{\theta_4}\int_{0}^{\varphi_{\max}} t_1'' \sin\theta d\varphi d\theta$	$\rho > R_a$
$\theta_c' > \theta_{cap}$	$\int_{\theta_1}^{\theta_c}\int_{0}^{\varphi_{\max}'} t_2'' \sin\theta d\varphi d\theta + \int_{\theta_{cap}}^{\theta_c'}\int_{0}^{\varphi_{\max}'} t_1'' \sin\theta d\varphi d\theta + \int_{\theta_c'}^{\theta_c}\int_{0}^{\varphi_c} t_1'' \sin\theta d\varphi d\theta + \int_{\theta_c}^{\theta_4}\int_{0}^{\varphi_{\max}} t_1'' \sin\theta d\varphi d\theta$	
$\theta_{cap} \ge \theta_c'$	$\int_{\theta_1}^{\theta_c'}\int_{0}^{\varphi_{\max}'} t_2'' \sin\theta d\varphi d\theta + \int_{\theta_c'}^{\theta_{cap}}\int_{0}^{\varphi_c} t_2'' \sin\theta d\varphi d\theta + \int_{\theta_{cap}}^{\theta_c}\int_{0}^{\varphi_c} t_1'' \sin\theta d\varphi d\theta + \int_{\theta_c}^{\theta_4}\int_{0}^{\varphi_{\max}} t_1'' \sin\theta d\varphi d\theta$	
$\theta_4 > \theta_{cap} \ge \theta_c$	$\int_{\theta_1}^{\theta_c'}\int_{0}^{\varphi_{\max}'} t_2'' \sin\theta d\varphi d\theta + \int_{\theta_c'}^{\theta_c}\int_{0}^{\varphi_c} t_2'' \sin\theta d\varphi d\theta + \int_{\theta_c}^{\theta_{cap}}\int_{0}^{\varphi_{\max}} t_2'' \sin\theta d\varphi d\theta + \int_{\theta_{cap}}^{\theta_4}\int_{0}^{\varphi_{\max}} t_1'' \sin\theta d\varphi d\theta$	
$\theta_{cap} \ge \theta_4$	$\int_{\theta_1}^{\theta_c'}\int_{0}^{\varphi_{\max}'} t_2'' \sin\theta d\varphi d\theta + \int_{\theta_c'}^{\theta_c}\int_{0}^{\varphi_c} t_2'' \sin\theta d\varphi d\theta + \int_{\theta_c}^{\theta_{cap}}\int_{0}^{\varphi_{\max}} t_2'' \sin\theta d\varphi d\theta + \int_{\theta_{cap}}^{\theta_4}\int_{0}^{\varphi_{\max}} t_1'' \sin\theta d\varphi d\theta$	

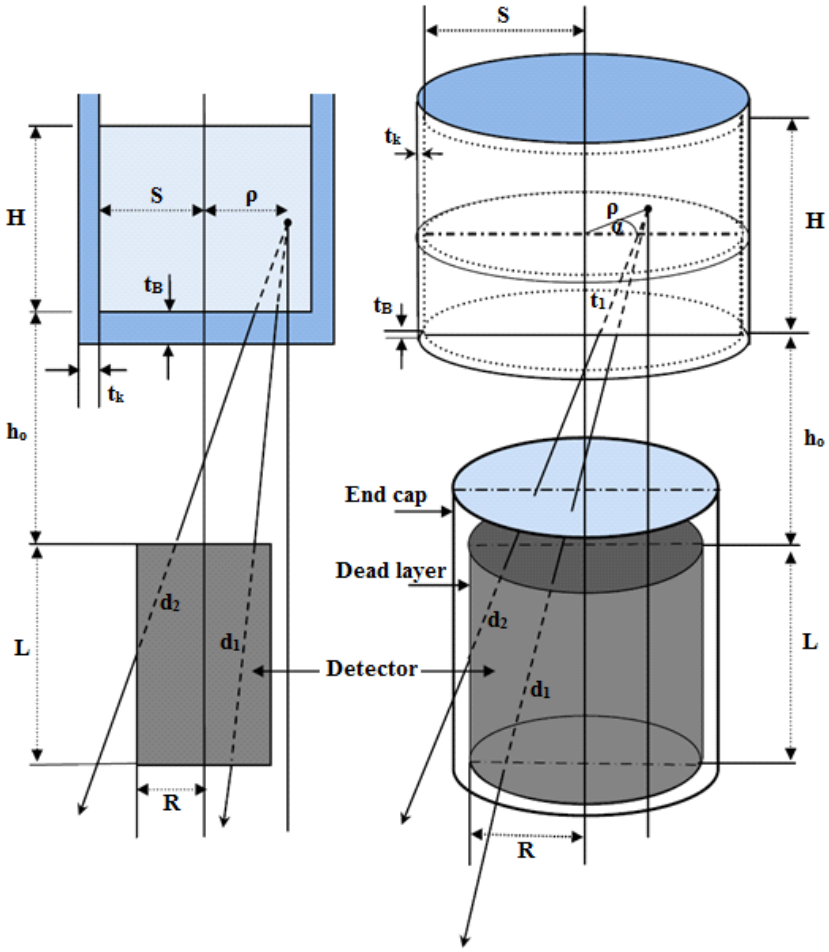

Fig. 2. The possible cases of the photon path lengths through source – detector system

container material and $\overline{t_c}$ is the average path length traveled by a photon inside the source container and is expressed as:

$$\overline{t_c} = \bar{t}(t_1''') . \qquad (37)$$

3. Experimental setup

The full-energy peak efficiency was measured for a p-types Canberra HPGe cylindrical detector (Model GC1520) with relative efficiency 15 %. Table 4 shows the manufacturer parameters in millimeter and the setup values for the detector. The sources are Polypropylene (PP) plastic vials of volumes 200 and 400 mL filled with an aqueous solution contains ^{152}Eu radionuclide which emits γ-ray in the energy range from 121 up to 1408 keV, Table 5 shows sources dimensions. Efficiency measurements were generated by positioning the sources over the end cap of the detector. In order to prevent dead time, the activity of the sources was kept low (5048 ± 49.98 Bq). Measurements were carried out using multichannel analyzers (MCA) to obtain statistically significant main peaks in the spectra that were recorded and processed by ISO 9001 Genie 2000 data acquisition and analysis software made by Canberra.

The acquisition time was high enough to make the statistical uncertainties less than 1%. The peaks were fitted using Gaussians with low-energy tails appropriate for germanium detector. Spectra acquired with gamma vision were analyzed with the program using its automatic peak search and peak area calculations, along with changes in the peak fit using the interactive peak fit interface when necessary to reduce the residuals and error in the peak area values. The peak areas, the live time, the run time and the start time for each spectrum were entered in the spreadsheets that were used to perform the calculations necessary to generate the efficiency curves.

Table 4. The manufacturer parameters and the setup values

Manufacturer	Canberra Industries	Drawing
Serial Number	06089367	
Detector Model	GC1520	
Geometry	Closed end Coaxial	
Relative Efficiency (%)	15	
Photopeak – Compton ratio	40	
Voltage bias (V)	(+) 4500	
Crystal Model	7500SL	
Resolution (FWHM) at 133 keV	2.0 keV	
Shaping time (ms)	4	
Preamplifier Model	2002CSL	
Amplifier Model	2026	
MCA	Multi port II	
VPS Model	3106D	
Detector type	HPGe (P- type)	
Shaping Model	Gaussian	
Mounting	Vertical	
Outer Electrode Thickness (mm)	0.5	
Inner Electrode Thickness (mm)	$0.3x10^{-3}$	
Window Electrode Thickness (mm)	0.5	
Crystal Diameter (mm)	48	
Crystal Length (mm)	54.5	
Core hole Diameter (mm)	7.5	
Core hole Depth (mm)	37.5	

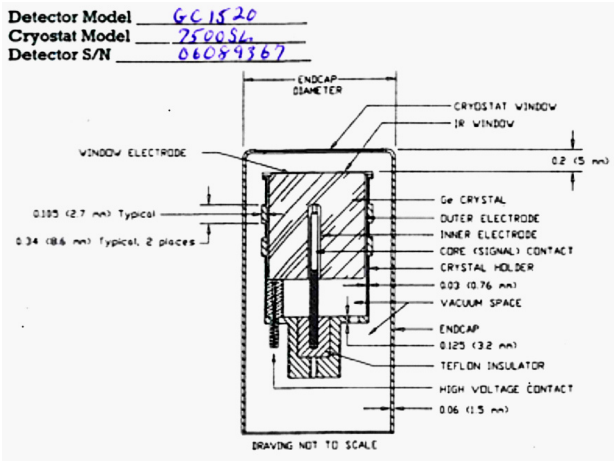

Table 5 Parameters of the sources

Source Volume mL		Items
400	**200**	
113.89	113.89	Outer diameter (mm)
42.25	21.13	Height (mm)
2.03	2.03	Wall thickness (mm)
5048 ± 49.98	5048 ± 49.98	Activity (Bq)

4. Results and discussion

The full-energy peak efficiency values for the p-type HPGe cylindrical type detector were measured as a function of the photon energy using the following equation

$$e(E) = \frac{N(E)}{T\ A_S\ P(E)} \prod C_i \qquad (38)$$

where N(E) is the number of counts in the full-energy peak which can be obtained using Genie 2000 software, T is the measuring time (in second), P(E) is the photon emission probability at energy E, A_S is the radionuclide activity and C_i are the correction factors due to dead time and radionuclide decay. In these measurements of low activity sources, the dead time always less than 3%, so the corresponding factor was obtained simply using ADC live time. The acquisition time was long enough to get statistical uncertainties of the net peak areas smaller than 1%. The background subtraction was done. The decay correction C_d for the calibration source from the reference time to the run time was given by:

$$C_d = e^{\lambda \Delta T} \qquad (39)$$

where λ is the decay constant and ΔT is the time interval over which the source decays corresponding to the run time. The main source of uncertainty in the efficiency calculations was the uncertainties of the activities of the standard source solutions. Once the efficiencies have been fixed by applying the correction factors; the overall efficiency curve is obtained by fitting the experimental points to a polynomial logarithmic function of the fifth order using a non linear least square fit. In this way, the correlation between data points from the same calibrated source has been included to avoid the overestimation of the uncertainty in the measured efficiency. The uncertainty in the full-energy peak efficiency σ_ε was given by:

$$y_e = e\sqrt{\left(\frac{\partial e}{\partial A}\right)^2 y_A{}^2 + \left(\frac{\partial e}{\partial P}\right)^2 y_P{}^2 + \left(\frac{\partial e}{\partial N}\right)^2 y_N{}^2} \qquad (40)$$

where σ_A, σ_P and σ_N are the uncertainties associated with the quantities A_S, P(E) and N(E) respectively. Figs. 3 and 4 show the full-energy peak efficiencies of a co-axial HPGe detector; measured, calculated with S_{self} and calculated without S_{self} for cylindrical sources (200 mL and 400 mL) as functions of the photon energy. Obviously, the neglected of the self attenuation factor in the calculations caused the increasing in the full energy peak efficiency values, so to get correct results; the self attenuation factor must be taken into consideration. The percentage deviations between the calculated (with and without S_{self}) and the measured full-energy peak efficiency values were calculated by:

$$Д_1\ \% = \frac{e_{\text{cal-with } S_{self}} - e_{meas}}{e_{\text{cal-with } S_{self}}} \times 100 \qquad (41)$$

$$Д_2\ \% = \frac{e_{\text{cal-without } S_{self}} - e_{meas}}{e_{\text{cal-without } S_{self}}} \times 100 \qquad (42)$$

where $\varepsilon_{\text{cal-with Sself}}$, $\varepsilon_{\text{cal-without Sself}}$ and ε_{meas} are the calculated with self attenuation factor, calculated without self attenuation factor and experimentally measured efficiencies, respectively. Figs. 5 and 6 show the percentage deviations Δ_1% and Δ_2% for cylindrical sources (200 mL and 400 mL respectively), placed at the end cap of p-type HPGe cylindrical detector.

According to Eq. (31), the self attenuation factor is depending on two important factors which are the attenuation coefficient of the source matrix and the average path length through the source itself. The effect of these factors can be shown in Fig. 7 which represents the variation of a self attenuation factor obtained from Eq. (31) with the photon energy. The self attenuation factor for 200 mL is greater than that of 400 mL when the two sources are placed at the same position with respect to the same detector; this is because the average path length calculated for 200 mL is smaller than that for 400 mL. So as the cylindrical source volume is increasing, the importance of the self attenuation factor becomes interesting and can't be neglected when calibrating the detector, but must be calculated with more accuracy to get good results. Also, the self attenuation is increasing as the energy is increasing and that is related to the effect of the source matrix attenuation coefficient.

5. Conclusions

In this work, the authors have derived direct mathematical expression for the calculation of the full-energy peak efficiency of a co-axial HPGe detector using a cylindrical source. The measurements were carried out by using ^{152}Eu aqueous radioactive source placed in large cylindrical beakers. Figs. 3–6 show there is a good agreement between the measured and the calculated values. The percentage deviations of the results are less than 2% when the self attenuation factor is taken into consideration.

22.03.2013

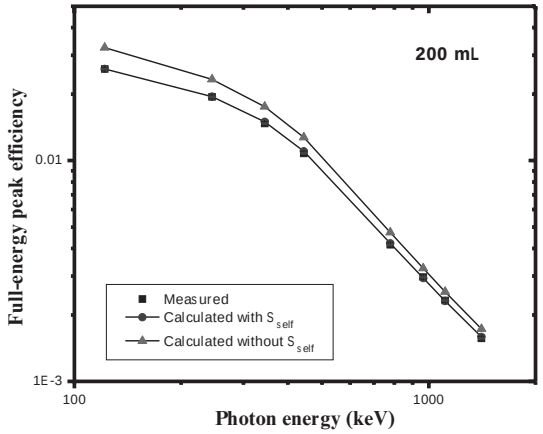

Fig. 3. The full-energy peak efficiencies of a co-axial HPGe detector; measured (squares and intervals), calculated with S_{self} (circles with solid line) and calculated without S_{self} (triangles with solid line) for cylindrical source (200 mL) as functions of the photon energy

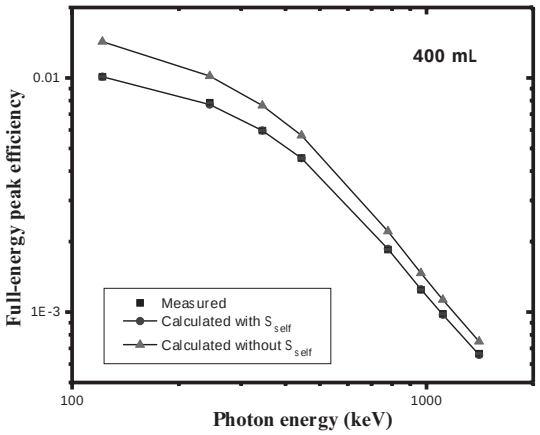

Fig. 4. The full-energy peak efficiencies of a co-axial HPGe detector; measured (squares and intervals), calculated with S_{self} (circles with solid line) and calculated without S_{self} (triangles with solid line) for cylindrical source (400 mL) as functions of the photon energy

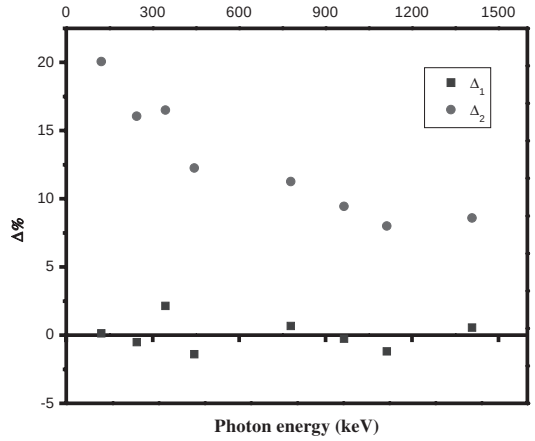

Fig. 5. The percentage deviations $Д_1$% and $Д_2$% for cylindrical source (200 mL) placed at the end cap of p-type HPGe cylindrical detector

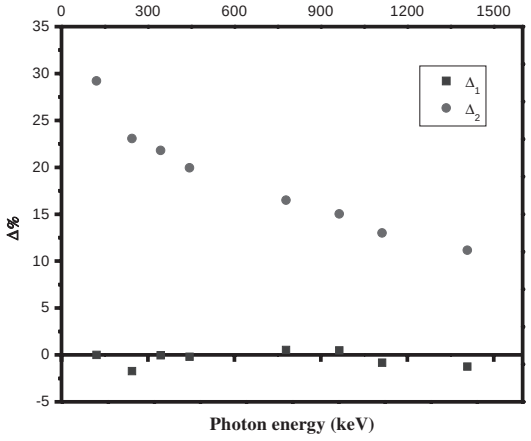

Fig. 6. The percentage deviations $Д_1$% and $Д_2$% for cylindrical source (400 mL) placed at the end cap of p-type HPGe cylindrical detector

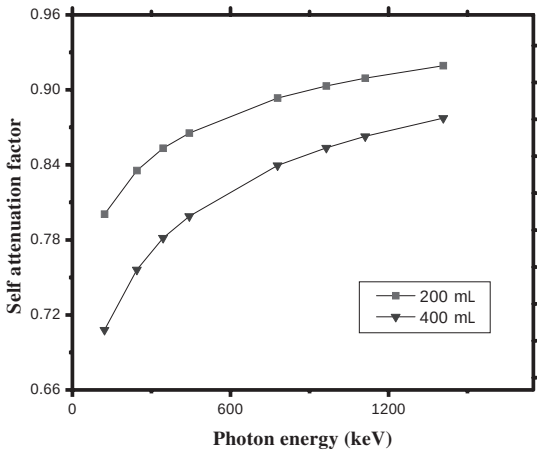

Fig. 7. Variation of self attenuation factor with the photon energy for different source volumes placed at the end cap of the detector

Acknowledgment

The authors would like to express their sincere thanks to Prof. Dr. Mahmoud. I. Abbas, Faculty of Science, Alexandria University, for the very valuable professional guidance in the area of radiation physics and for his fruitful scientific collaborations on this topic.

Dr. Mohamed. S. Badawi would like to introduce a special thanks to The Physikalisch-Technische Bundesanstalt (PTB) in Braunschweig, Berlin, Germany for fruitful help in preparing the homemade volumetric sources.

References:

1. Abbas, M.I., 2001a. A direct mathematical method to calculate the efficiencies of a parallelepiped detector for an arbitrarily positioned point source. Radiat. Phys. Chem. 60, 3.
2. Abbas, M.I., 2001b. Analytical formulae for well-type NaI(Tl) and HPGe detectors efficiency computation. Appl. Radiat. Isot. 55, 245.
3. Abbas, M.I., 2001c. HPGe detector photopeak efficiency calculation including self-absorption and coincidence corrections for Marinilli beaker sources using compact analytical expressions. Appl. Radiat. Isot. 54, 761.
4. Abbas, M.I., Younis,Y. S., 2002. Calculation of relative full-energy peak efficiencies of well-type detectors. Nucl. Instrum. Methods A 480, 651.
5. Abbas, M.I., 2006. HPGe detector absolute full-energy peak efficiency calibration including coincidence correction for circular disc sources. J. Phys. D: Appl. Phys. 39, 3952.
6. Abbas, M.I., Nafee, S.S., Selim, Y.S., 2006. Calibration of cylindrical detectors using a simplified theoretical approach. Appl. Radiat. Isot. 64, 1057.
7. Haase, G., Tait, D., Wiechon, A., 1993. Application of new Monte Carl method for determination of summation and self-attenuation corrections in gamma spectrometry. Nucl. Instrum. Methods A336 ,206.
8. Lippert, J., 1983. Detector-efficiency calculation based on point-source measurement. Int. J. Appl. Radiat. Isot. 34, 1097.
9. Mihaljevic, N., De Corte, S., De Corte, F., Smodis, B., Jacimovic, R., Medin, G., De Wispelaere, A., Vukotic, P., Stegner, P., 1993. J. Radioanal. Nucl. Chem. 169, 209.
10. Moens, L., De Donder, J., Lin, X. L., De Corte, F., De Wispelaere, A., Simonits, A., Moens, L., Hoste, J., 1983. Calculation of the peak efficiency of high-purity germanium detectors. Int. J. Appl. Radiat. Isot. 34, 1085.
11. Nakamura, T., 1983. Monte Carlo calculation of peak efficiencies of Ge(Li) and pure Ge detectors to voluminal sources and comparison with environmental radioactivity measurement. Nucl. Instrum. Methods 205, 211.
12. Nafee, S.S., Abbas, M.I., 2008. Calibration of closed-end HPGe detectors using bar (parallelepiped) sources. Nucl. Instrum. Methods A 592, 80.
13. Selim, Y.S., Abbas, M.I., 1995. Direct calculation of the total efficiency of cylindrical scintillation detectors for non-axial point sources. Egypt. J. Phys. 26, 79.
14. Selim, Y.S., Abbas, M.I., 1996. Direct calculation of the total efficiency cylindrical scintillation detectors for extended circular sources. Radiat. Phys. Chem. 48, 23.
15. Selim, Y.S., Abbas, M.I., Fawzy, M.A., 1998. Analytical calculation of the efficiencies of gamma scintillators. Part I: total efficiency of coaxial disk sources. Radiat. Phys. Chem. 53, 589.
16. Selim, Y.S., Abbas, M.I., 2000. Analytical calculations of gamma scintillators efficiencies. Part II: total efficiency for wide coaxial disk sources. Radiat. Phys. Chem. 58, 15.
17. Sima, O., Arnold, D., 1996. Self-attenuation and coincidence summing corrections calculated by Monte Carlo simulations for gamma-spectrometric measure- ments with well-type germanium detectors. Appl. Radiat. Isot. 47, 889.
18. Wang, T.K., Mar, W.Y., Ying, T.H., Liao, C.H., Tseng, C.L., 1995. HPGe detector absolute-peak-efficiency calibration by using the ESOLAN program. Appl. Radiat. Isot. 46, 933.
19. Wang, T.K., Mar, W.Y., Ying, T.H., Tseng, C.H., Liao, C.H., Wang, M.Y., 1997. HPGe Detector efficiency calibration for extended cylinder and Marinelli- beaker sources using the ESOLAN program. Appl. Radiat. Isot. 48, 83.

M. S. Badawi, Physics Department, Faculty of Science, Alexandria University, 21511 Alexandria, Egypt. [Doctor], e-mail: ms241178@hotmail.com, Tel:+201005154976.

M. M. Goud, Physics Department, Faculty of Science, Alexandria University, 21511 Alexandria, Egypt. [Doctor], e-mail: ahec3@yahoo.com, Tel:+201142911711.

A. M. El-Khatib, Physics Department, Faculty of Science, Alexandria University, 21511 Alexandria, Egypt. [Professor. Doctor], e-mail: Elkhatib60@yahoo.com, Tel:+201000230122.

S. S. Nafee, Physics Department, Faculty of Science, Alexandria University, 21511 Alexandria, Egypt. [Doctor], e-mail: nafee_shra@yahoo.com, Tel:+201010058780.

E. A. El-Mallah, Physics Department, Faculty of Science, Alexandria University, 21511 Alexandria, Egypt. [Doctor], e-mail: ekramelmallah@yahoo.com, Tel:+201005154976.